Journal of Applied Geology, vol. 9(1), 2024, pp. 37–50
DOI: http://dx.doi.org/10.22146/jag.97467

Slope Stability Analysis Using Electrical Resistivity Tomography and Limit Equilibrium Method: A Case Study from Girimulyo, Kulon Progo

Putri Anjary Widya Santie[1], Wahyu Wilopo*[2], and Fikri Faris[1]

[1]*Civil and Environment Engineering Department, Faculty of Engineering, Universitas Gadjah Mada Yogyakarta*
[2]*Department of Geological Engineering, Faculty of Engineering, Universitas Gadjah Mada, Yogyakarta, Indonesia*

Received: June 24, 2024 | Accepted: September 18, 2024 | Published online: October 31, 2024

ABSTRACT. Girimulyo sub-district is one of the areas with high landslide risk in Kulon Progo Regency. On March 12, 2018, a landslide occurred in the area. Seven families were affected, and landslide material blocked the road. This study uses the limit equilibrium method to determine slope conditions through electrical resistivity tomography (ERT) and slope stability analysis. Based on the interpretation of the ERT profile, it is known that a layer with a resistivity value of <5 Ωm is wet clay; 5–15 Ωm is wet silt; 15-150 Ωm is silt-to-sand; and >150 Ωm is bedrock. The sliding surface is thought to be at the boundary between the damp clay and wet silt layers. The interpretation of the ERT profile is confirmed by data from laboratory tests on soil samples. Slope stability analysis was performed using ERT profile interpretation and soil sample laboratory test data. The slope stability analysis results show that both the slopes that experienced landslides in 2018 and those that did not experience landslides were stable when the water table was 3 meters deep. However, the landslide slopes are in critical condition as the groundwater level rises, while the non-landslide slopes remain stable.

Keywords: Electrical resistivity tomography · Landslide · Limit equilibrium method · Slope stability.

1 INTRODUCTION

Landslides have become Indonesia's third most common disaster in the last decade after floods and tornadoes. Kulon Progo is one of the districts where landslides often occur. The topography of the northern and central parts of Kulon Progo, consisting of hills, increases the region's vulnerability to landslide hazards. According to the Kulon Progo Regency Disaster Risk Assessment Document 2022–2026, 10.38 % of the area of Kulon Progo Regency is in the high hazard zone for landslides, while 36.14% of the area is in the moderate hazard zone (BPBD Kab. Kulon Progo, 2022). On March 12, 2018, a landslide occurred in Karanggede, Jatimulyo village, Girimulyo district, Kulon Progo Regency (Figure 1). The landslide was triggered by heavy rainfall, which caused the material on the slope to slide down. The landslide affected seven families and blocked the road, cutting off access between the Jatimulyo and Girimulyo villages. Considering the large number of people living there, it is important to evaluate the condition of the slopes in the Karanggede area.

ERT is a geophysical technique that measures the electrical properties of rock formations below the earth's surface by injecting electric current into the ground (Telford *et al.*, 1990). ERT is a geophysical method often used in landslide investigations (Perrone *et al.*, 2014). ERT can identify slope lithology, slope geometry, landslide type, location of failure zones or slip

*Corresponding author: W. WILOPO, Department of Geological Engineering, Faculty of Engineering, Universitas Gadjah Mada, Yogyakarta, Indonesia. E-mail: wilopo_w@ugm.ac.id

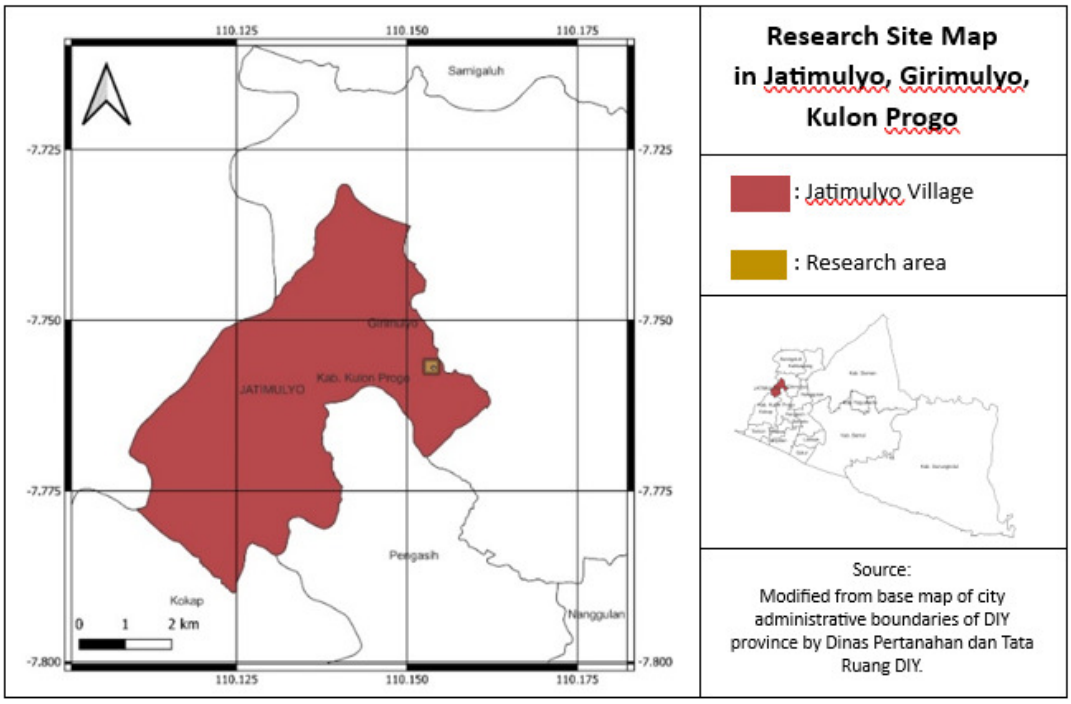

FIGURE 1. Research location where a landslide occurred on March 12, 2018, in Karanggede.

planes, differentiate between soil and bedrock boundaries, and identify areas of excess moisture (Asriza *et al.*, 2017; Chibani *et al.*, 2023; Crawford *et al.*, 2018; Imani *et al.*, 2021; Jianjun *et al.*, 2020; Kamiński *et al.*, 2023; Pasierb *et al.*, 2019; Usman *et al.*, 2020). ERT's results are instrumental in determining the spatial distribution of contacts between different materials. As a result, it is possible to obtain 2D geotechnical models of soil layers for slope stability analysis.

Once the stratigraphy of the soil layer on the slope is known, it is essential to understand its physical and mechanical properties. The soil's physical and mechanical properties influence the stability of the disturbed slope (Mugagga *et al.*, 2012). The slope stability analysis was performed based on the limit equilibrium method using Slope/W. The limit equilibrium method was chosen because it is widely used with easily selectable structural models and provides a clear mechanical concept for vector calculations, allowing rapid stability factor calculation (Wang *et al.*, 2023). This paper analyzes slope stability by integrating the ERT and limit equilibrium methods to obtain slope safety factors in Karanggede and evaluate slope conditions after the 2018 landslide. By knowing the slope's stability under various conditions, we can identify the external factors that influence the stability of the slope so that recommendations for appropriate slope management can be determined.

2 GEOLOGICAL SETTING/SITE CHARACTERIZATION

The geomorphology of the study area is characterized by the structural landscape of the cuestas (ridges of gentle and steep slopes) and by tectonic features such as faults and rifts. Geomorphic processes in the study area include fluvial activity and mass movement (Husein & Srijono, 2010). Based on the geological map of Yogyakarta, the research site is located in the Old Andesite Formation. Figure 2 shows the research site on the Yogyakarta geological map; the blue squares indicate the research sites.

Bemmelen gave the name of the Old Andesite Formation in 1949, which was later revised by Pringgoprawiro and Riyanto in 1987 into two formations, namely the Kaligesing Formation and the Dukuh Formation. The Kaligesing Formation is characterized by monomic breccia with andesite fragments, sandstone interbeds, and andesite lava. The Dukuh Formation comprises polymictic breccia with andesite, sandstone, and limestone fragments. The age of the formation is late Oligocene - early Miocene.

Based on the Kulon Progo Regency Soil

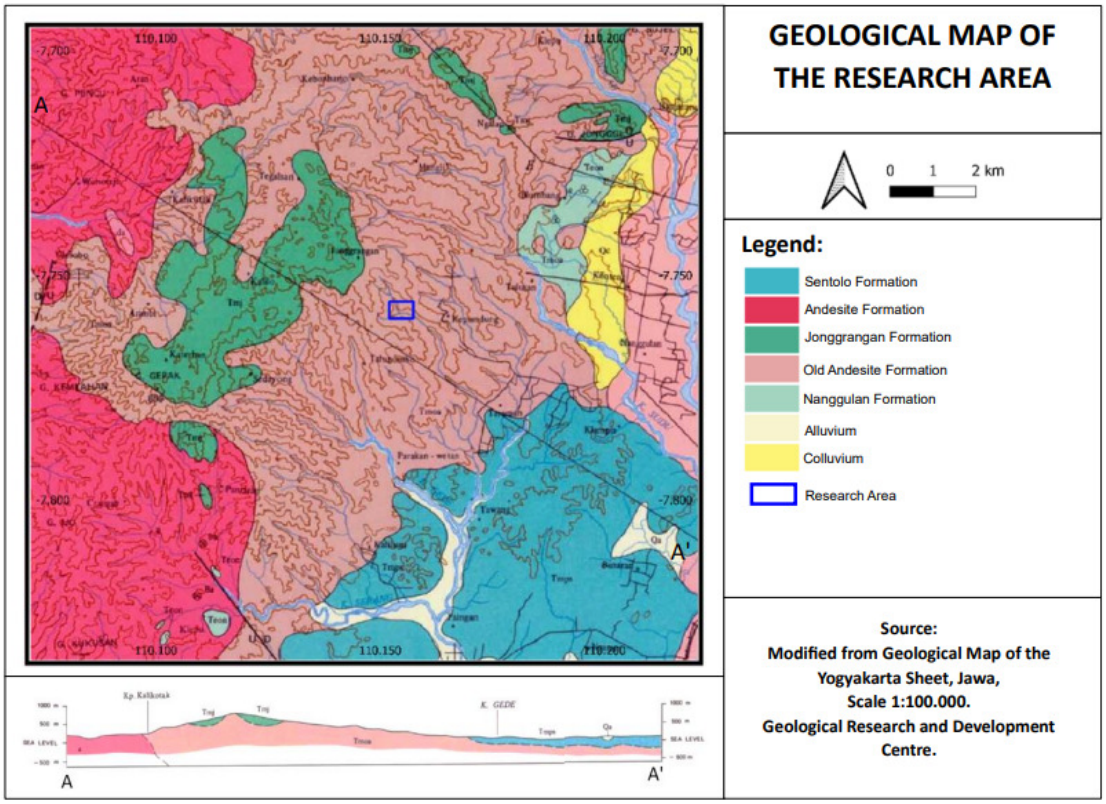

FIGURE 2. Geological setting of research location based on the geological map of Yogyakarta (Rahardjo *et al.*, 1977).

Type Map, the study area comprises latosol soil. Dudal and Supraptoharjo (1957) state that Latosol soil is highly weathered with low organic matter, primary minerals, and nutrients. Latosol soil has the characteristics of red, reddish brown to yellowish brown or yellow. Latosol is a type of soil with high clay content.

As shown in Figure 3, the landslide event in early March 2018 was preceded by high average monthly rainfall in January and February.

The average monthly precipitation in January and February 2018 reached 450 mm and 402 mm, respectively. Slope stability was significantly affected by rainfall and groundwater level fluctuations. Although the landslide hazard increases considerably during the rainy season, the movement of landslides also increases significantly after the middle of the rainy season (Anh Bui *et al.*, 2019). Increased load can trigger progressive movement due to accumulated mass groundwater inflow (Wilopo *et al.*, 2020).

3 METHODOLOGY

The research began by conducting preliminary investigations in literature studies to collect data and information related to ground motion at the research site and its geological and geomorphological conditions. Field investigations were conducted through geological investigations to map outcrops and geological structures at the research site, as well as mapping cracks and the location of springs at the research site. Based on the field investigation results, a data acquisition design was made.

3.1 Electrical Resistivity Tomography (ERT)

The ERT technique is based on the measurement of electrical resistivity. It can provide 2D and 3D images of its distribution in the subsurface. A model inversion uses an inversion routine to determine the true subsurface resistivity from the apparent resistivity values (Perrone et al., 2014). This study used the VES (1D) and profiling (2D) methods to collect electrical resistivity data. The VES method is carried out with the Schlumberger configuration, while the Profiling (2D) method is carried out

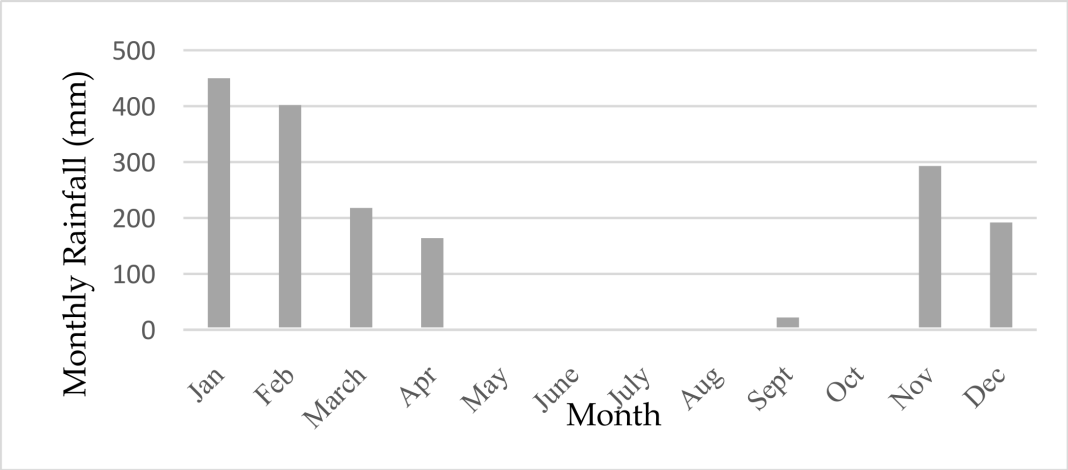

FIGURE 3. Monthly rainfall of Girimulyo district in 2018 (Badan Pusat Statistik Kabupaten Progo Kulon, 2019).

with the Wenner-Schlumberger configuration. Figure 4a. is the electrode arrangement for the Schlumberger configuration, while Figure 4b. is the electrode arrangement for the Wenner-Schlumberger configuration.

Calculated resistivity is not actual subsurface resistivity but apparent resistivity, where homogeneous soil gives the same resistivity for the same electrode arrangement. Resistivity meters typically provide a resistance value (R). In practice, the apparent resistivity value is calculated as follows

$$\rho_a = k \cdot R \tag{1}$$

Where ρ_a = Apparent Resistivity (Ωm), k = geometry factor, and R = Resistance (Ω).

The ERT profile for the slope at the research site was measured by measuring the 1D electrical resistivity (VES) at three points and the profiling (2D) at five lines. Geoelectric data acquisition was conducted in November 2023. Figure 5 shows the acquisition design for ERT and soil sampling. VES method was conducted at three points using the Schlumberger configuration. Meanwhile, 2D geoelectric measurements were performed on 5 lines using the Wenner-Schlumberger configuration with 5 m spacing.

3.2 Soil sampling and soil laboratory test

After obtaining the ERT profile, soil samples are collected to represent very low, low, and medium resistivity values. All three samples were collected using a hand auger to a depth of 2 m for samples A and B and 1 m for sample C. All three soil samples taken were undisturbed.

The undisturbed soil samples are tested in the laboratory to determine physical properties, including water content, Atterberg limits, unit weight, and grain size. Mechanical properties are determined by soil shear strength testing using triaxial Undrained-Unconsolidated (UU).

3.3 Slope stability analysis

Slope stability analysis was performed using the results of ERT profile interpretation and laboratory tests on soil samples. In this study, slope stability analysis was performed using the limit equilibrium method with Slope/W. The limit equilibrium method considers the final limit state and does not provide information about the strain development. In the case of natural slopes, a portion of the failure mass may experience such large stresses that residual forces will be mobilized at some locations. In contrast, the ultimate shear forces can be applied to other portions of the failure mass. This type of progressive failure can occur in overly consolidated or cracked clays or materials with brittle properties (Cheng & Lau, 2014).

The primary objective of most stability analyses is to determine the slope safety factor. A limit state of equilibrium is said to exist when the shear stress along the failure surface is expressed as:

$$F = \frac{\tau}{\tau_d} \tag{2}$$

where τ = shear stress, τ_d = shear strength,

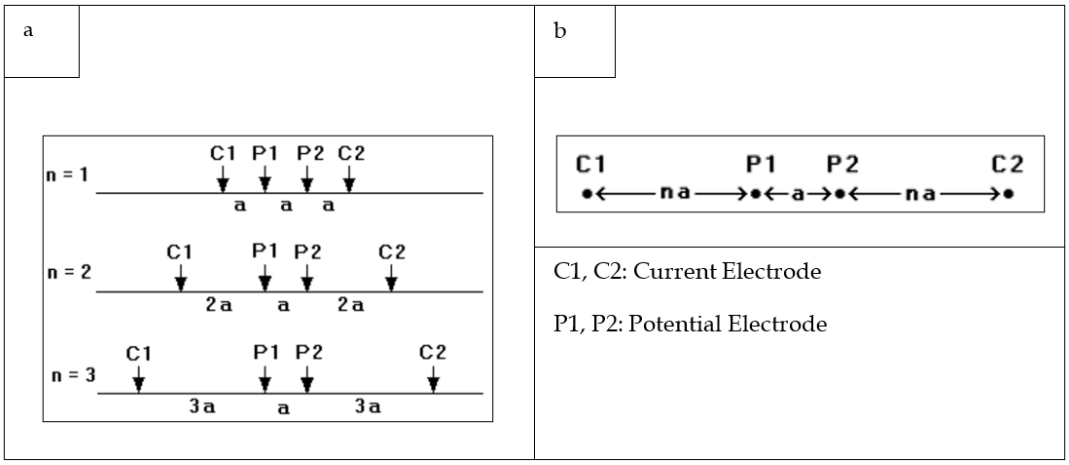

FIGURE 4. Electrode arrangement for ERT (a) Wenner-Schlumberger configuration, (b) Schlumberger configuration.

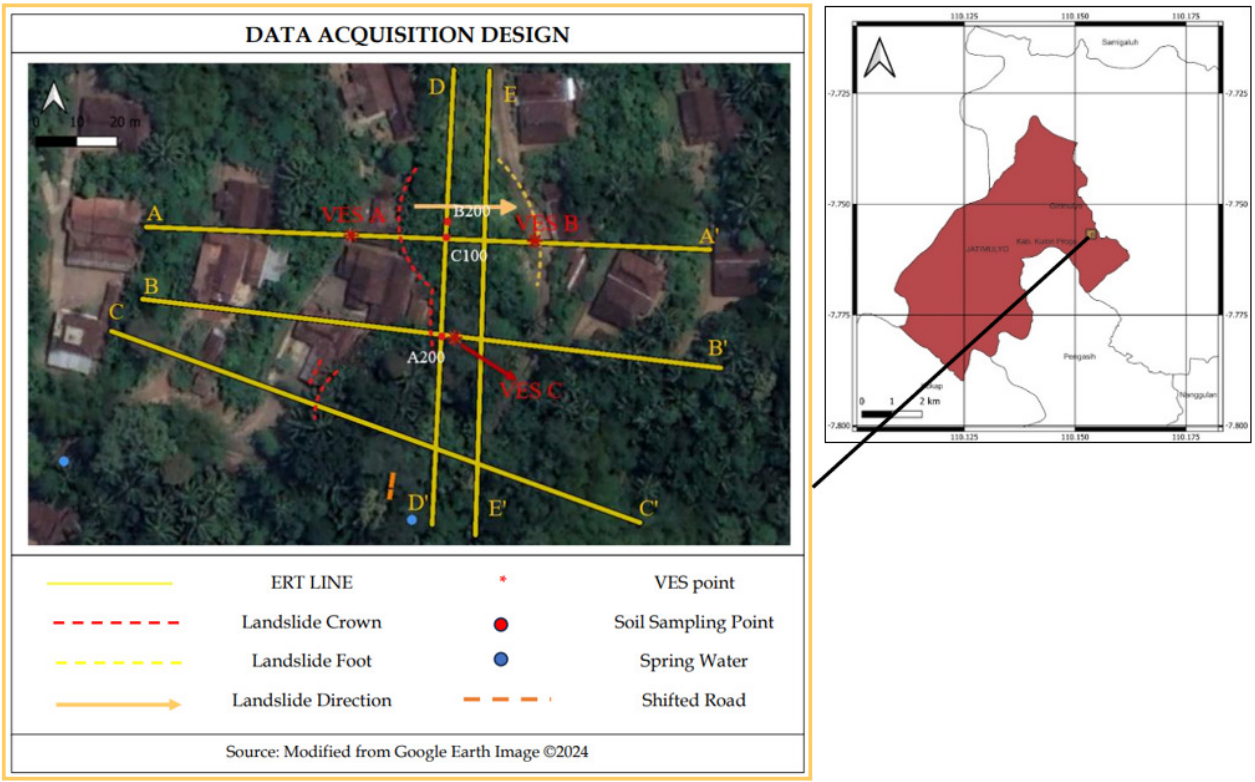

FIGURE 5. Data acquisition design.

and F = safety factor. According to Mohr-Coulomb failure theory, shear strength is expressed as:

$$\tau = c + \sigma \tan \phi \tag{3}$$

Meanwhile, the shear strength of the soil formed on the sliding surface of the landslide τ_d is given in the following equation:

$$\tau_d = c_d + \sigma \tan \phi_d \tag{4}$$

Where c_d and ϕ_d are the values of cohesion and internal friction angle, respectively. By substituting Equation 3 and Equation 4 into Equation 2, the equation for the safety factor is obtained as in the following equation:

$$F = \frac{c + \sigma \tan \phi}{c_d + \sigma \tan \phi_d} \tag{5}$$

The Morgenstern-Price method is a limit equilibrium calculation method that satisfies the balance of forces and moments and assumes a force function between slices. In several slope stability analysis studies, the FS (factor of safety) value plays an important role in determining the significance of slope stability. Table 1. does Bowles give the factor of safety value.

TABLE 1. Safety Factor of Slope (Bowles, 1979).

Safety Factor	Slope Condition
FS < 1.07	Unstable
1.07 < FS < 1.25	Critical
FS > 1.25	Stable

4 RESULTS AND DISCUSSION

Based on the curve matching of the VES data (Figure 6), the results are shown in Table 2. The graph is a plot between spacing (AB/2) and the apparent resistivity value. The resistivity value for each layer is obtained from the curve fitting results.

Figure 6 shows the relationship between inverted and synthetic data. The blue curve is the model parameter that can be changed in curve fitting, the black curve is the observation curve describing the field data, and the red curve is the model calculation data. Smaller errors mean that observations will be closer to computations. Figure 6a is the result of curve matching for VES A with an error of 3.11%. Figure 6b is the result of curve matching for VES B with an error of 2.54 % and Figure 6c is the result of curve matching for VES C with an error of 3.88%

Figures 7–10 show the 2D ERT profiles for the five lines and their geological interpretation. Figure 7 is the ERT profiles for line A–A′. This line passed through a slope that experienced a landslide in 2018. The red dashed line shows the location of the landslide crown, while the yellow dashed line shows the landslide foot. It can be seen in the ERT A–A′ profile that there is a very low resistivity (<5 Ωm) layer at 5–10 meters. The low resistivity layer is interpreted as wet clay between the wet silt layers (5–15 Ωm). A medium resistivity (15–150 Ωm) layer of silt-to-sand overlies these two layers. The slip surface on this line is predicted to be at the boundary between the wet clay and wet silt layers.

Figure 8 is the ERT profiles for line B-B′. Lines A–A′ and B–B′ passed through the crown of the landslide in 2018. Both lines show similar profiles. After the crown of the landslide, there is a layer of very low resistivity (<5 Ωm) between low resistivity values (5–15 Ωm). The very low resistivity layer is interpreted as wet clay between the wet silt layers. A medium resistivity (15–150 Ωm) layer of silt-to-sand overlies these two layers. The slip surface on both lines is predicted to be at the boundary between the wet clay and wet silt layers, where both layers are saturated with water.

Unlike the A–A′ and B–B lines, the C–C′ line does not pass through the crown of the 2018 landslide. Instead, it shows signs of movement in the form of longitudinal cracks. In Figure 9, it can be seen that there is an andesite intrusion near the surface, which is indicated by a high resistivity value (>150 Ωm). As in the two previous lines, the C–C′ line was also found to have very low resistivity (<5 Ωm), indicated as wet clay, and between layers of low resistivity (5–15 Ωm), marked as wet silt. The boundary between the wet clay and wet silt layers is predicted to be a possible sliding surface.

The D–D′ and E–E′ lines have different directions from the three previous lines. The D–D′ and E–E′ lines are perpendicular to the direction of the landslide. The predicted slip sur-

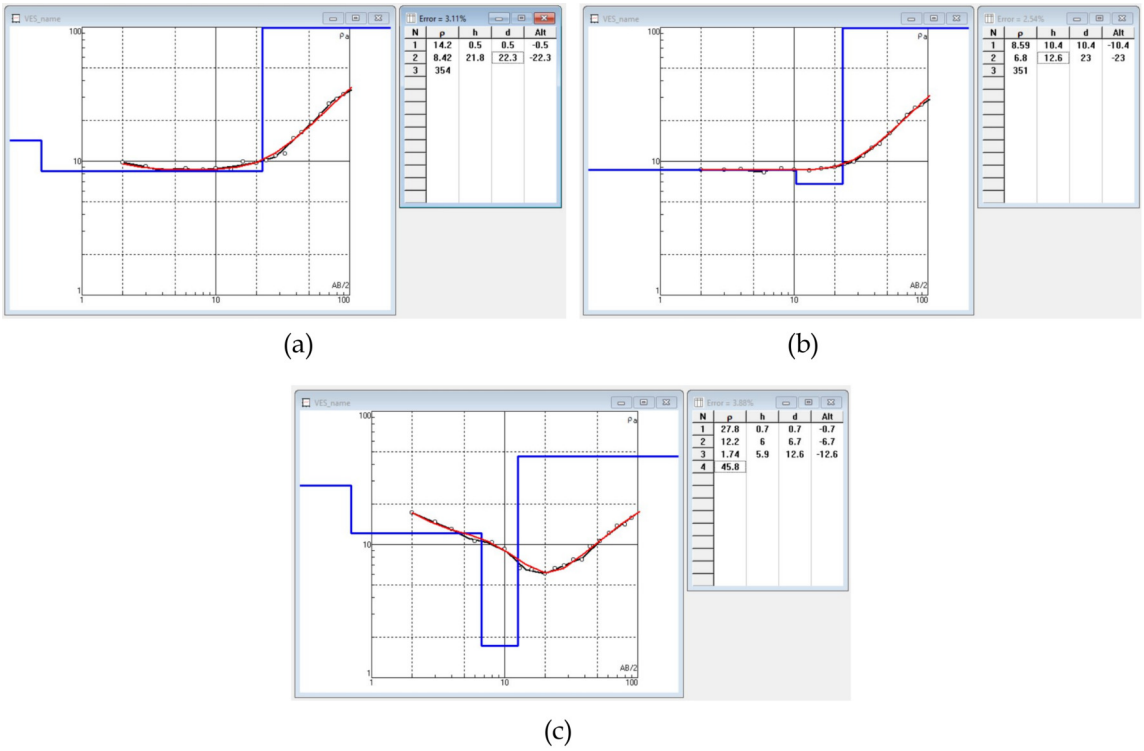

FIGURE 6. (a) Curve Matching VES A, (b) Curve Matching VES B, (c) Curve Matching VES C.

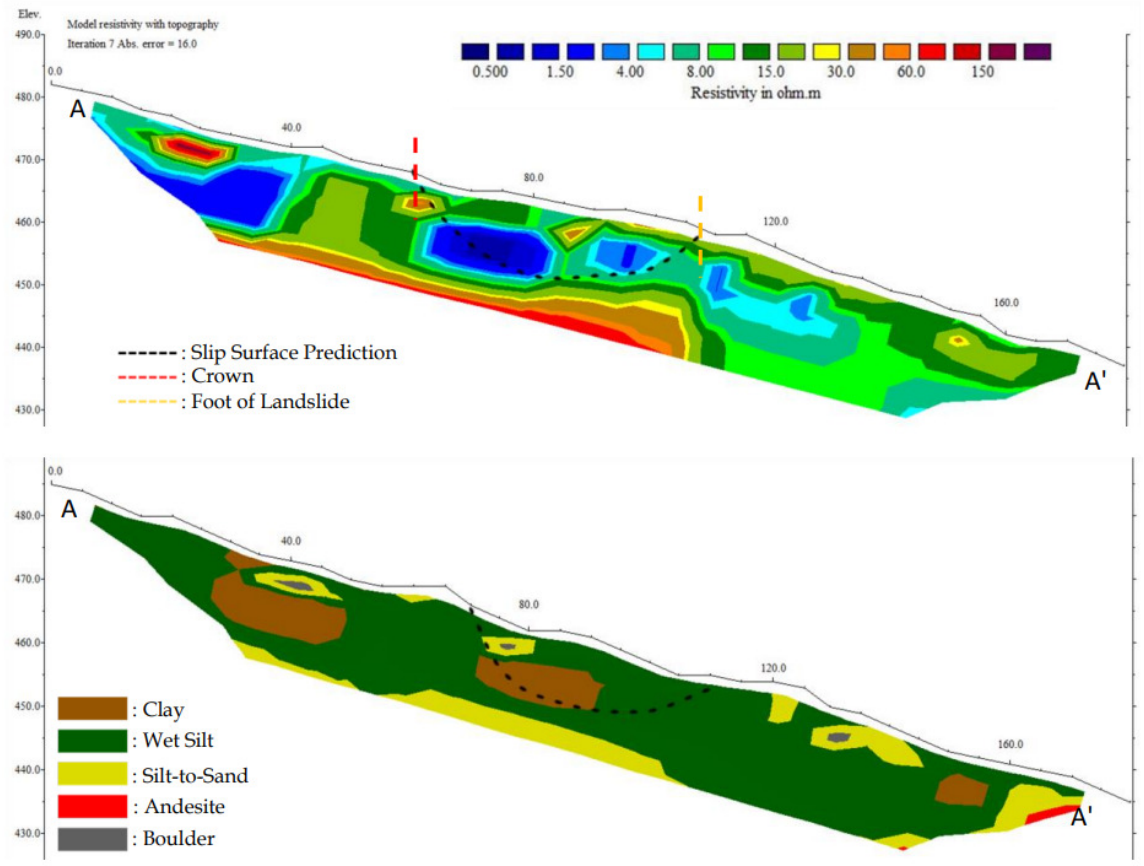

FIGURE 7. ERT profiles and geological interpretation for lines A–A′.

TABLE 2. VES curve matching interpretation.

VES A			VES B			VES C		
Resisti-vity	Depth (m)	Interpre-tation	Resisti-vity	Depth (m)	Interpre-tation	Resisti-vity	Depth (m)	Interpre-tation
14.2	0–0.5	Wet silt	14.2	0–0.5	Wet silt	14.2	0–0.5	Wet silt
8.42	0.5–22.3	Wet silt	8.42	0.5–22.3	Wet silt	8.42	0.5–22.3	Wet silt
354	>22.3	Andesite	354	>22.3	Andesite	354	>22.3	Andesite

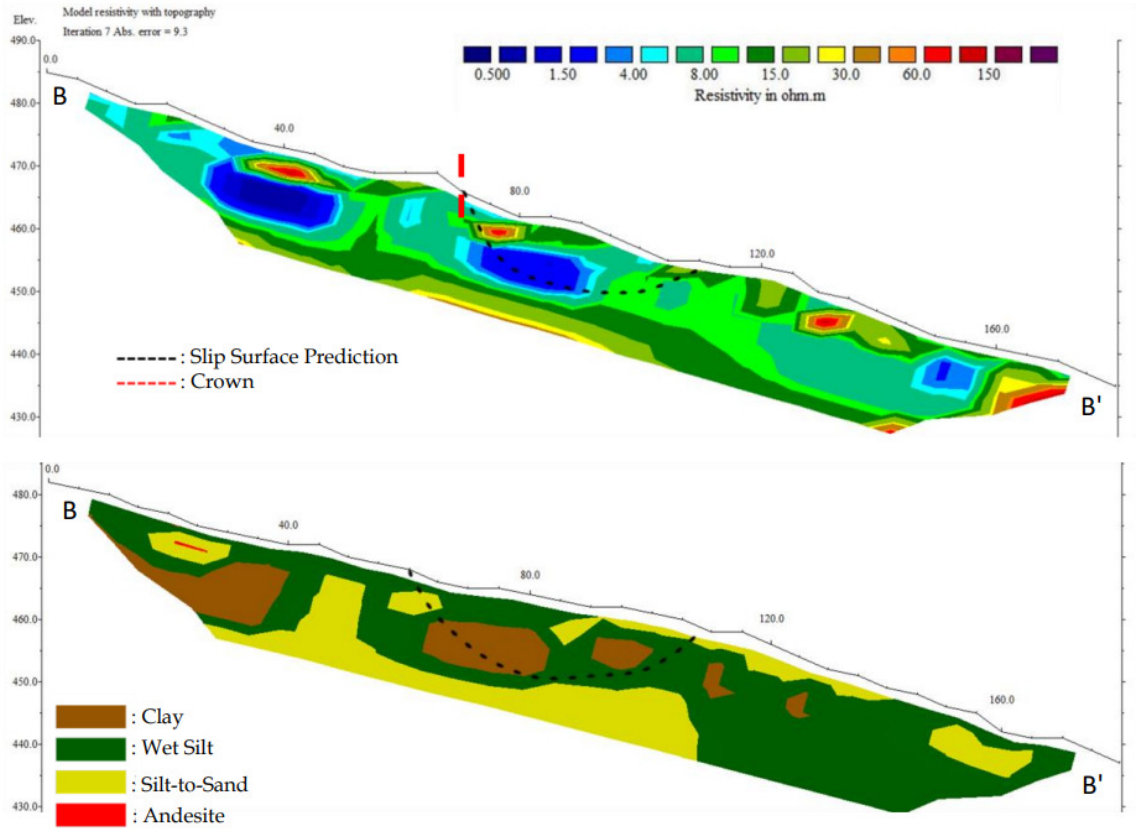

FIGURE 8. ERT profiles and geological interpretation for lines B–B′.

face of lines A–A′ and B–B′ can be confirmed using the ERT profile of the D–D′ line. In the D–D′ line (Figure 10), a very low resistive layer (<5 Ωm), interpreted as a layer of wet clay, lies above a low resistive layer (5–15 Ωm), interpreted as a layer of wet silt. The boundary between the two layers is considered to be the slip surface. Below these two layers is a layer with medium resistivity (15–150 Ωm), which is interpreted as a silt-to-sand.

Line E–E′ (Figure 11) is close to the foot of the landslide, no slip surface was found on this line. The E–E′ band is dominated by a low resistivity layer (5–15 Ωm) interpreted as wet silt. A moderate resistivity layer (15–150 Ωm) was also found and interpreted as silt-to-sand.

A correlation was made between the 2D ERT profile and the VES resistivity log to obtain deeper layers. VES A and B are on the ERT A–A′ line. Figure 12a. the correlation between VES A and B with ERT line A–A′ shows that at 22 meters in VES A and 23 meters in VES B, there is a layer with high resistivity values, interpreted as bedrock. Figure 12b is the correlation of VES C with ERT line B–B′.

This correlation confirms the presence of a layer of wet clay between the layers of wet silt overlying the layer of silt to sandy. Based on the ERT profile, soil samples are taken and tested in the laboratory. Laboratory test results for soil samples from the research site are presented in Table 3.

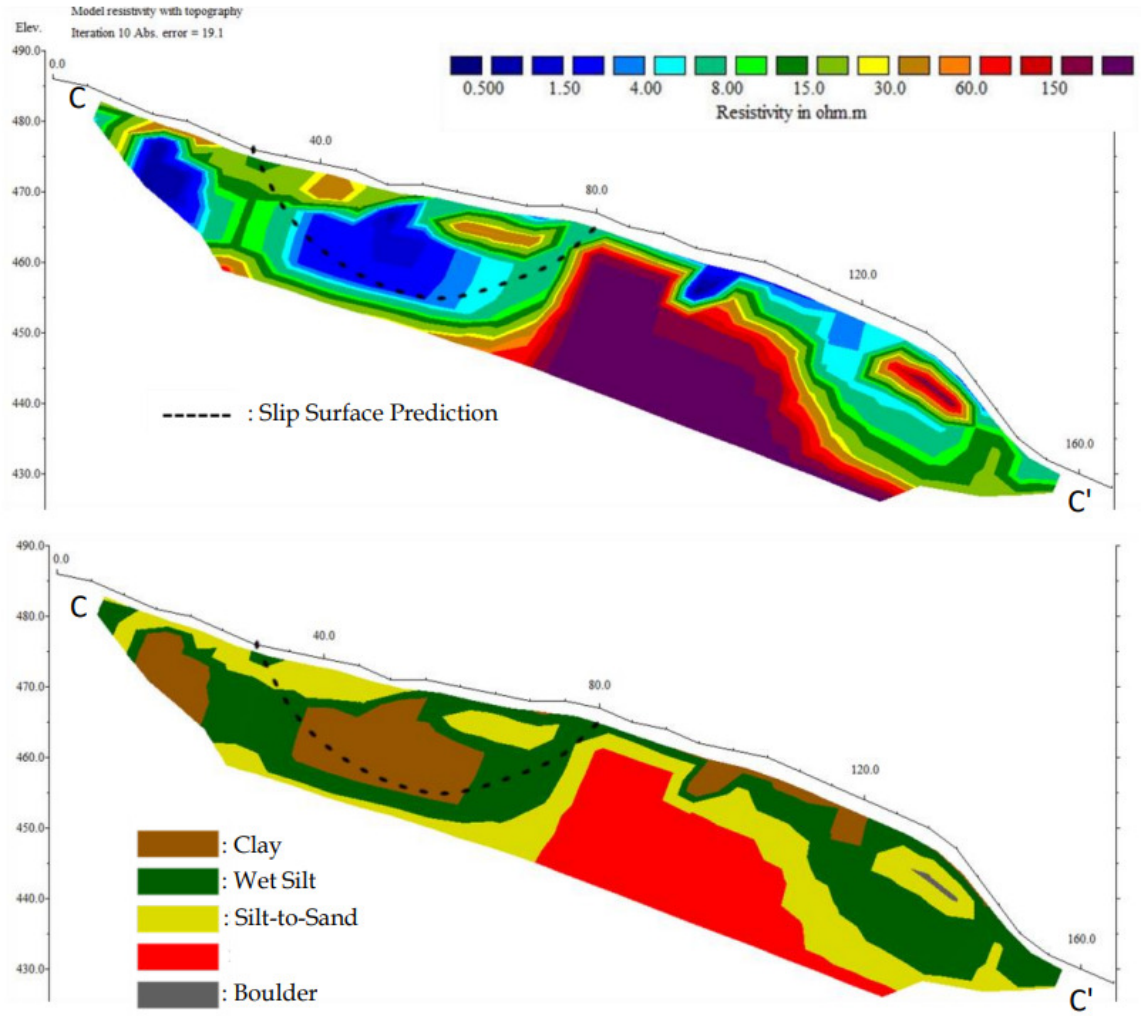

FIGURE 9. ERT profiles and geological interpretation for line C–C′.

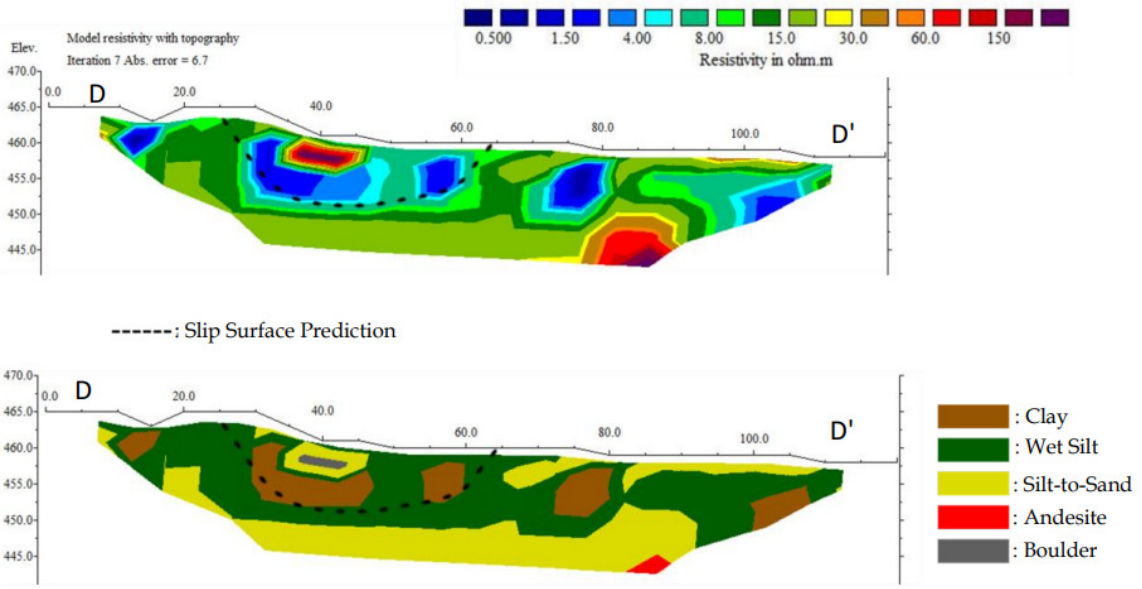

FIGURE 10. ERT profiles and geological interpretation for line D–D′.

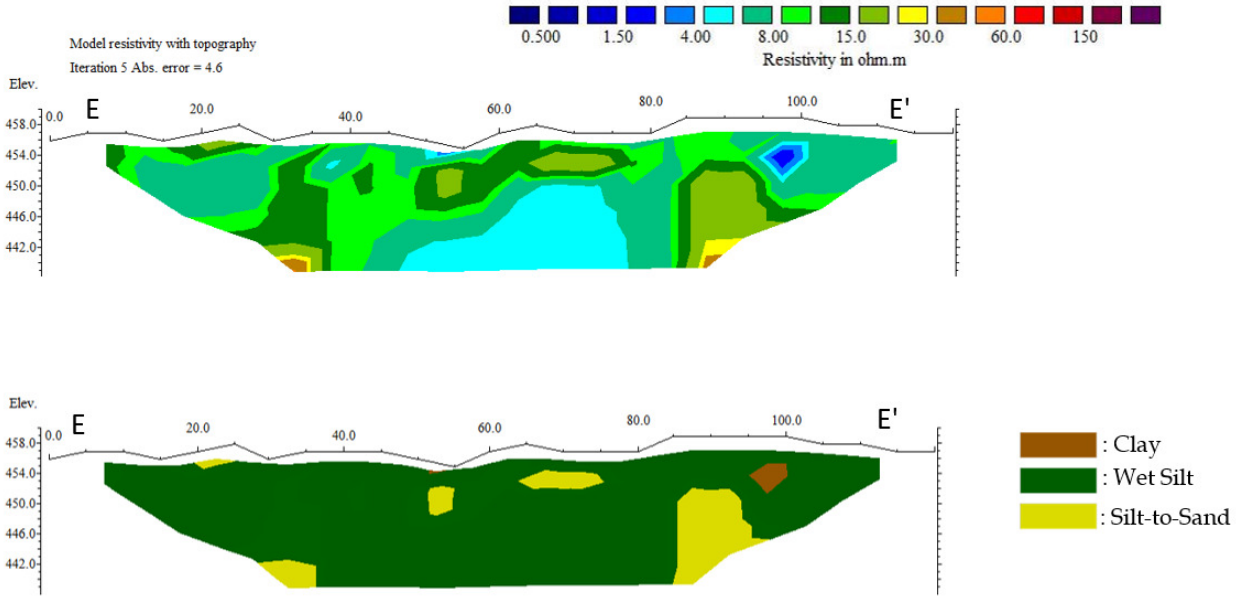

FIGURE 11. ERT profiles and geological interpretation for line E–E′.

TABLE 3. Laboratory test result on soil sample.

Code	Grain Size Distribution					Index Properties						Mech. Prop.	
	Gravel %	Sand %	Silt %	Clay %	Wn %	γ_d kN/m^3	γ_b kN/m^3	LL %	PL %	PI %	LI	c °	ϕ kN/m^2
A	2.58	9.95	33.89	53.57	52.98	10.8	16.5	67.1	32.68	34.42	0.59	4.92	27.2
B	0	16.24	38.03	45.73	52.69	10.7	16.3	51.71	31.12	20.6	1.05	9.17	25.4
C	2.16	22.58	37.05	38.21	50.94	10.9	16.4	55.39	33.15	22.24	0.8	7.13	60.5

Based on the grain size distribution results in Table 3, it can be seen that the three soil samples belong to the fine-grained soil, as >50 % of the grains pass the 200 sieve. The three samples contain relatively high natural water levels, over 50%. Furthermore, the three samples show that the soil at the research site is highly plastic. It has a plasticity index of >17. Then, the soil type can be determined for each sample using the USCS soil classification system. Since the three samples are fine-grained soils with liquid limit ≥50, the plasticity graph must be plotted by entering liquid limit (LL) and plasticity index (PI) values.

Based on plotting results on the plasticity graph in Figure 13 and grain size distribution in Table 3, soil samples A, B, and C are high plasticity clay, elastic silt, and elastic silt with sand. The correlation between the ERT profile interpretation and the USCS soil classification results is shown in Table 4. It can be seen that there is a good agreement between the understanding of the ERT profile and the soil classification results based on the soil sample tests.

Slope stability analysis was performed using Slope/W using geometric input based on geologic interpretation of A–A′ and B–B′ lines, physical and mechanical parameter input from soil sample test results.

Figure 14 is the result of the slope stability analysis. Although it passed through the same crown of landslides, unlike the A–A′ slope, the slope along the ERT B–B′ line did not experience landslides in 2018. A slope stability analysis was conducted to compare both slopes at the same condition.

Figure 14a and b are the initial analysis conditions for slope A–A′ and slope B–B′; when the water table is at a depth of 3 m, it is seen that the slope safety factor is 1.344 and 1.802, which means that the slope is in a stable condition. As the water table rises until the slope is fully sat-

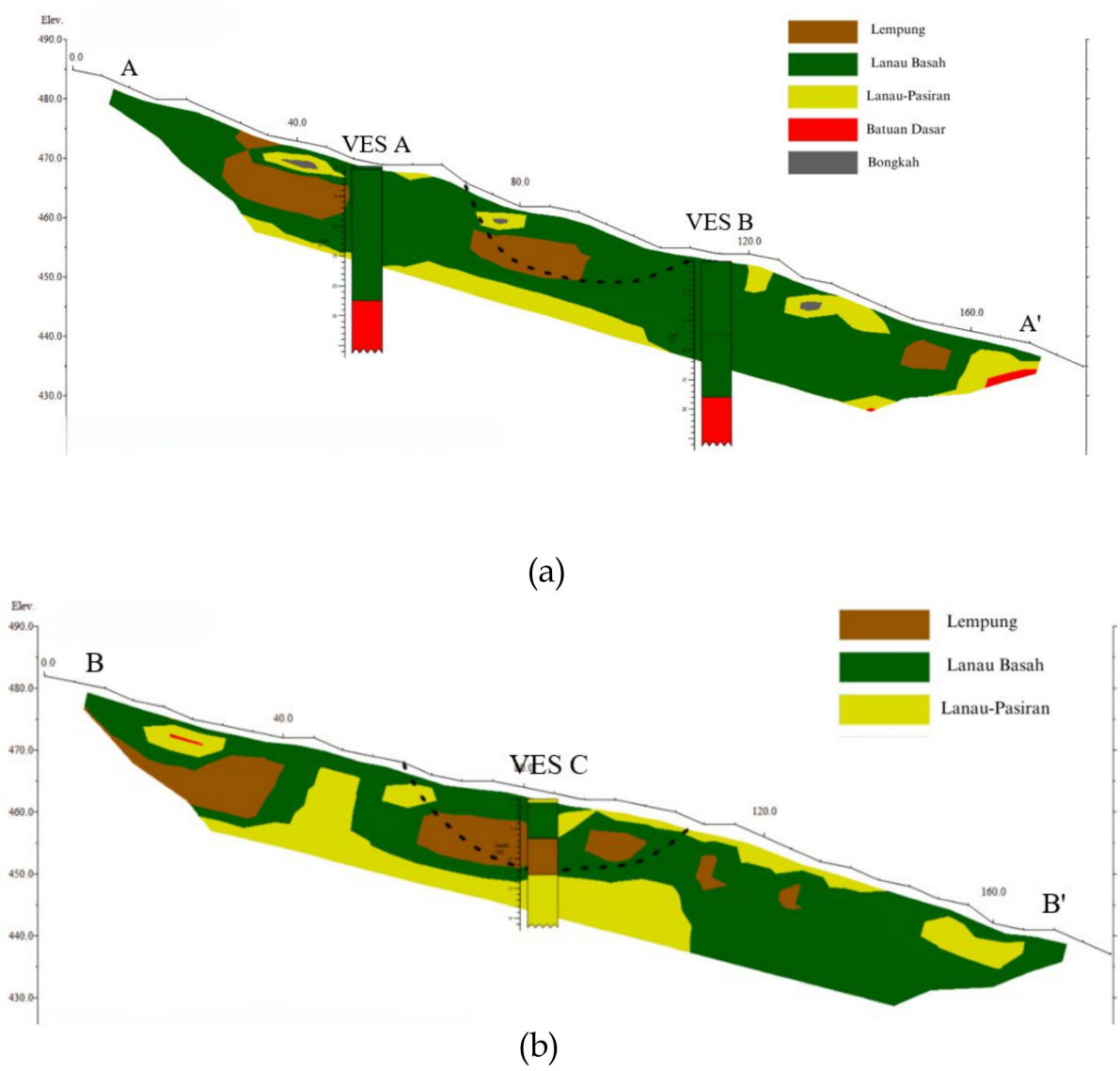

FIGURE 12. (a) Correlation between VES A and B with ERT line A–A′, (b) Correlation between VES C with ERT line B–B′.

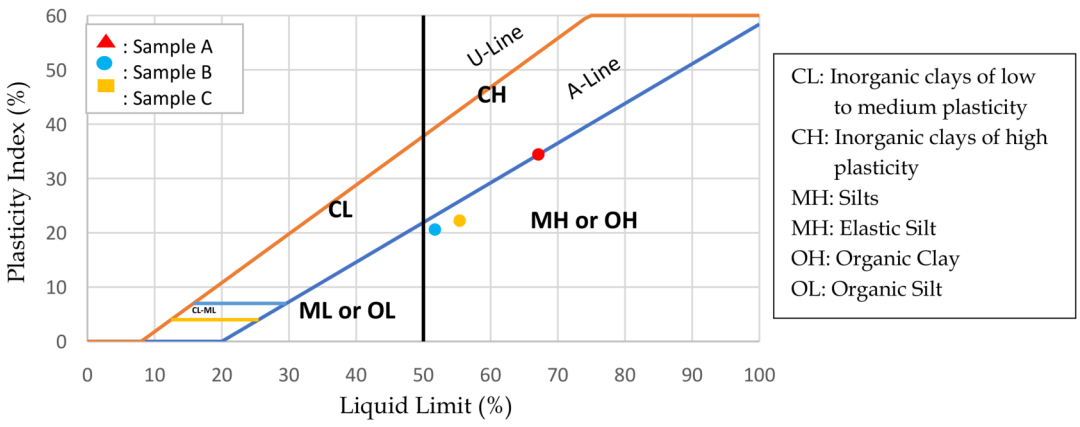

FIGURE 13. USCS soil classification plasticity chart.

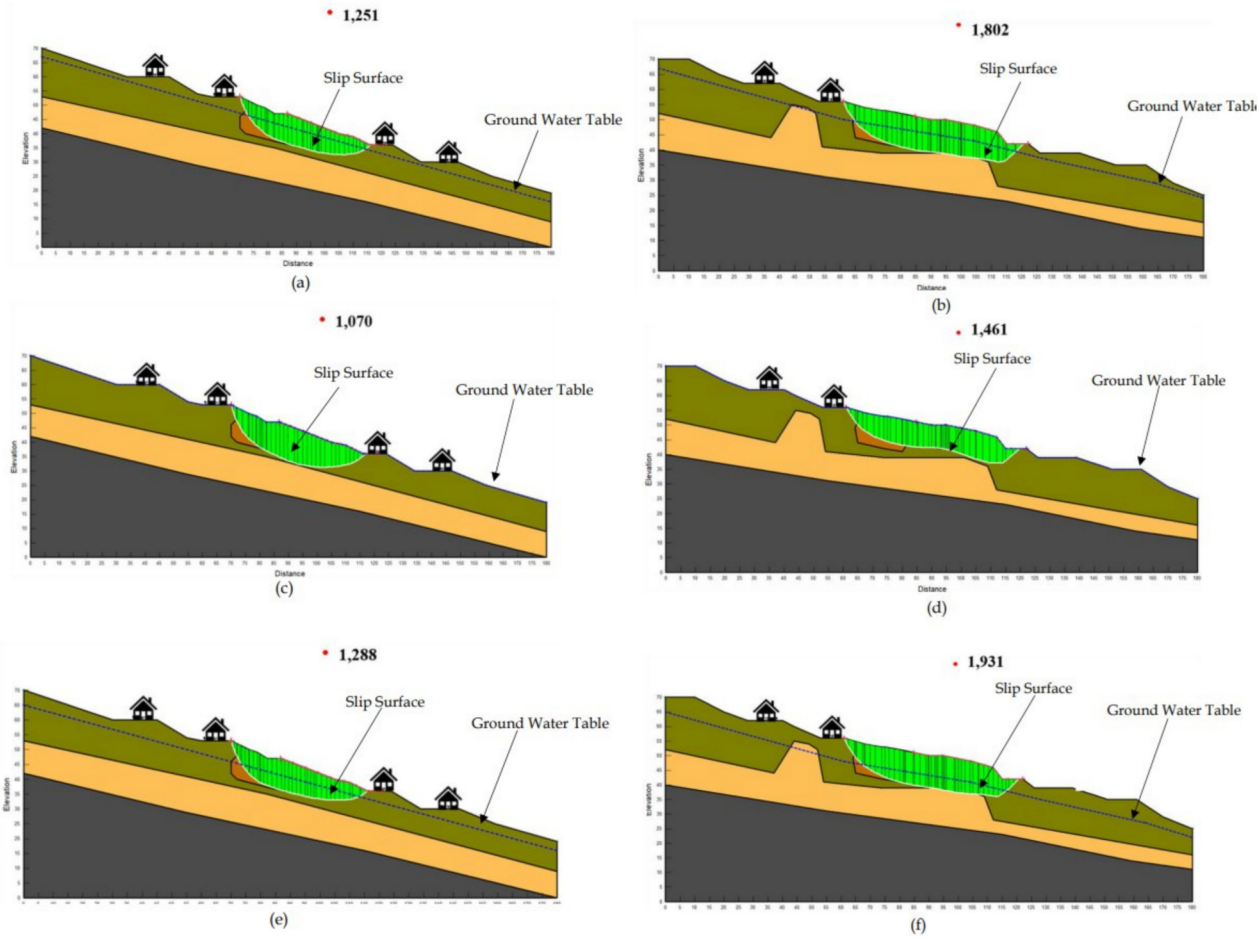

Colour	Material	c (kN/m^2)	ϕ (°)	γ (kN/m^3)
	Clay	27.2	4.92	16.5
	Silt	25.4	9.17	16.3
	Silt-to-Sand	60.5	7.13	16.4
	Andesite	-	-	-

FIGURE 14. (a) The slope stability analysis results of the initial condition (GWT=3m) A–A′ slope, (b) The slope stability analysis results of the initial condition (GWT=3m) B–B′ slope, (c) Results of slope stability analysis when GWT rises in A–A′ slope, (d) Results of slope stability analysis when GWT rises in B–B′ slope, (e) Results of the slope stability analysis of the initial condition (GWT=5m) A–A′ slope, (f) Results of the slope stability analysis of the initial condition (GWT=5m) B–B′ slope.

TABLE 4. The correlation between the ERT profile interpretation and the USCS soil classification.

Code	Resistivity	Type of Soil Based on ERT	Kind of Soil Based on USCS
A	<5 Ωm	Wet Clay	High Plasticity Clay
B	5–15 Ωm	Wet Silt	Elastic Silt
C	15–150 Ωm	Silt to Clay	Elastic Silt with Sand

urated with water, as in Figure 14c and d, the slope safety factor drops to 1.185 for slope A–A′ and 1.461 for slope B–B′. The safety factor value indicates the slope is critical and prone to landslides for slopes A-A′, while slopes B–B′ remain stable.

To see the effect of the groundwater level on the slope safety factor, an analysis is performed by lowering the groundwater level by 2 m from the initial condition. At a groundwater level of 5 m (Figure 14e, the slope safety factor is 1.424, indicating stability for A–A′ slope. Figure 14f shows the result of the stability analysis of slope B-B′ for the same conditions. It can be seen that the safety factor of slope B–B′ when the groundwater level is 5 m deep is 1.931, which indicates that the hill is in stable condition.

The results indicate that, under the same conditions, slope B–B′ provides a higher slope safety factor than slope A–A′. Additionally, there is a similarity in the slip surface of the landslide at the study site, as observed from the ERT profile and slope stability analysis

5 CONCLUSION

This study integrated geoelectrical and geotechnical methods to assess the slope conditions in Karanggede after the 2018 landslide. Based on the ERT profile, the sliding surface of the landslide at the study site likely lies at the interface between wet clay and wet silt. The results of the slope stability analysis indicate that both the slopes that experienced landslides in 2018 and those that did not were stable when the groundwater level was at a depth of 3 meters. However, as the water table rises, the slopes that experienced landslides become critical, while the slopes that did not experience landslides remain stable. The stability of both slopes was increased by lowering the water table.

REFERENCES

Anh Bui, T., Fathani, T. F., & Wilopo, W. (2019). Landslide Risk Assessment for Designing Monitoring and Early Warning System. *Journal of Applied Geology*, 4(1), 1. DOI: 10.22146/jag.48735.

Asriza, Supriyanto, Kristyanto, T. H. W., Indra, T. L., Syahputra, R., & Tempessy, A. S. (2017). Determination of the Landslide Slip Surface Using Electrical Resistivity Tomography (ERT) Technique. In Advancing Culture of Living with Landslides (pp. 53–60). Springer International Publishing. DOI: 10.1007/978-3-319-53498-5_7.

Badan Pusat Statistik Kabupaten Progo Kulon. (2019). KABUPATEN KULON PROGO DALAM ANGKA (Kulon Progo Regency in Figures) 2019.

Bowles, J. E. (1979). Physical and Geotechnical Properties of Soil. McGraw-Hill.

BPBD Kab. Kulon Progo. (2022). KAJIAN RISIKO BENCANA KABUPATEN KULON PROGO TAHUN 2022-2026.

Cheng, Y. M., & Lau, C. K. (2014). Slope stability analysis and stabilization: new methods and insight (2nd ed.). CRC Press Taylor & Francis Group.

Chibani, A., Hebbache, K., Mellas, M., & Mabrouki, A. (2023). 2D electrical resistivity tomography (ERT) investigation of a landslide: A case study from Ali Mendjeli, Constantine, North-East of Algeria. *NRIAG Journal of Astronomy and Geophysics*, 12(1), 45–57. DOI: 10.1080/20909977.2022.2163787.

Crawford, M. M., Bryson, L. S., Woolery, E. W., & Wang, Z. (2018). Using 2-D electrical resistivity imaging for joint geophysical and geotechnical characterization of shallow landslides. *Journal of Applied Geophysics*, 157, 37–46. DOI: 10.1016/j.jappgeo.2018.06.009.

Husein, S., & Srijono. (2010). Peta Geomorfologi Daerah Istimewa Yogyakarta. Simposium Geologi Yogyakarta. DOI: 10.13140/RG.2.2.10627.50726.

Imani, P., Tian, G., Hadiloo, S., & El-Raouf, A. A. (2021). The application of combined electrical resistivity tomography (ERT) and seismic refraction tomography (SRT) methods to investigate the Xiaoshan District landslide site in Hangzhou, China. *Journal of Applied Geophysics*, 184. DOI: 10.1016/j.jappgeo.2020.104236.

Jianjun, G., Zhang, Y. X., & Xiao, L. (2020). Applying the high-density electrical resistivity method for detecting slide zones in deep-seated landslides in limestone areas. *Journal of Applied Geophysics*, 177. DOI: 10.1016/j.jappgeo.2020.104013.

Kamiński, M., Zientara, P., & Krawczyk, M. (2023). Application of airborne laser scanning and electrical resistivity tomography in studying an active landslide and geology of the cliff, Jastrzębia Góra, Poland. *Bulletin of Engineering Geology and the Environment*, 82(4). DOI: 10.1007/s10064-023-03153-z.

Mugagga, F., Kakembo, V., & Buyinza, M. (2012). A characterization of the physical properties of soil and the implications for landslide occurrence on the slopes of Mount Elgon, Eastern Uganda. Natural Hazards, 60(3), 1113–1131. DOI: https://doi.org/10.1007/s11069-011-9896-3.

Pasierb, B., Grodecki, M., & Gwóźdź, R. (2019). Geophysical and geotechnical approach to a landslide stability assessment: a case study. *Acta Geophysica*, 67(6), 1823–1834. DOI: 10.1007/s11600-019-00338-7.

Perrone, A., Lapenna, V., & Piscitelli, S. (2014). Electrical resistivity tomography technique for landslide investigation: A review. *Earth-Science Reviews*, 135, pp. 65–82. DOI: 10.1016/j.earscirev.2014.04.002.

Rahardjo, W., Sukandarrumidi, & Rosidi, H.M.D. (1977). Peta Geologi Lembar Yogyakarta, Jawa. Direktorat Geologi.

Telford W.M, Geldart L.P, & Sheriff R.E. (1990). Applied Geophysics (2nd ed.). Cambridge University Press. DOI: 10.1017/CBO9781139167932.

Usman, F. C. A., Manyoe, I. N., Duwingik, R. F., & Kasim, D. N. P. (2020). Geophysical survey of landslide movement and mechanism in Gorontalo Outer Ring Road, Gorontalo. *IOP Conference Series: Earth and Environmental Science*, 589(1). DOI: 10.1088/1755-1315/589/1/012008.

Wang, Y., Li, Y., & Chen, J. (2023). Comprehensive Analysis Method of Slope Stability Based on the Limit Equilibrium and Finite Element Methods and Its Application. *Open Journal of Civil Engineering*, 13(04), 555–571. DOI: 10.4236/ojce.2023.134040.

Wilopo, W., Setiawan, H., Prakasa Eka Putra, D., & Faisal Fathani, T. (2020). Identification of Sliding Surface and Crack Pattern in the Soil Creep, Case Study: Unika Soegijapranata Campus, Semarang, Central Java, Indonesia. Understanding and Reducing Landslide Disaster Risk, 4, 451–457. DOI: 10.1007/978-3-030-60706-7_48.